Fig.S1

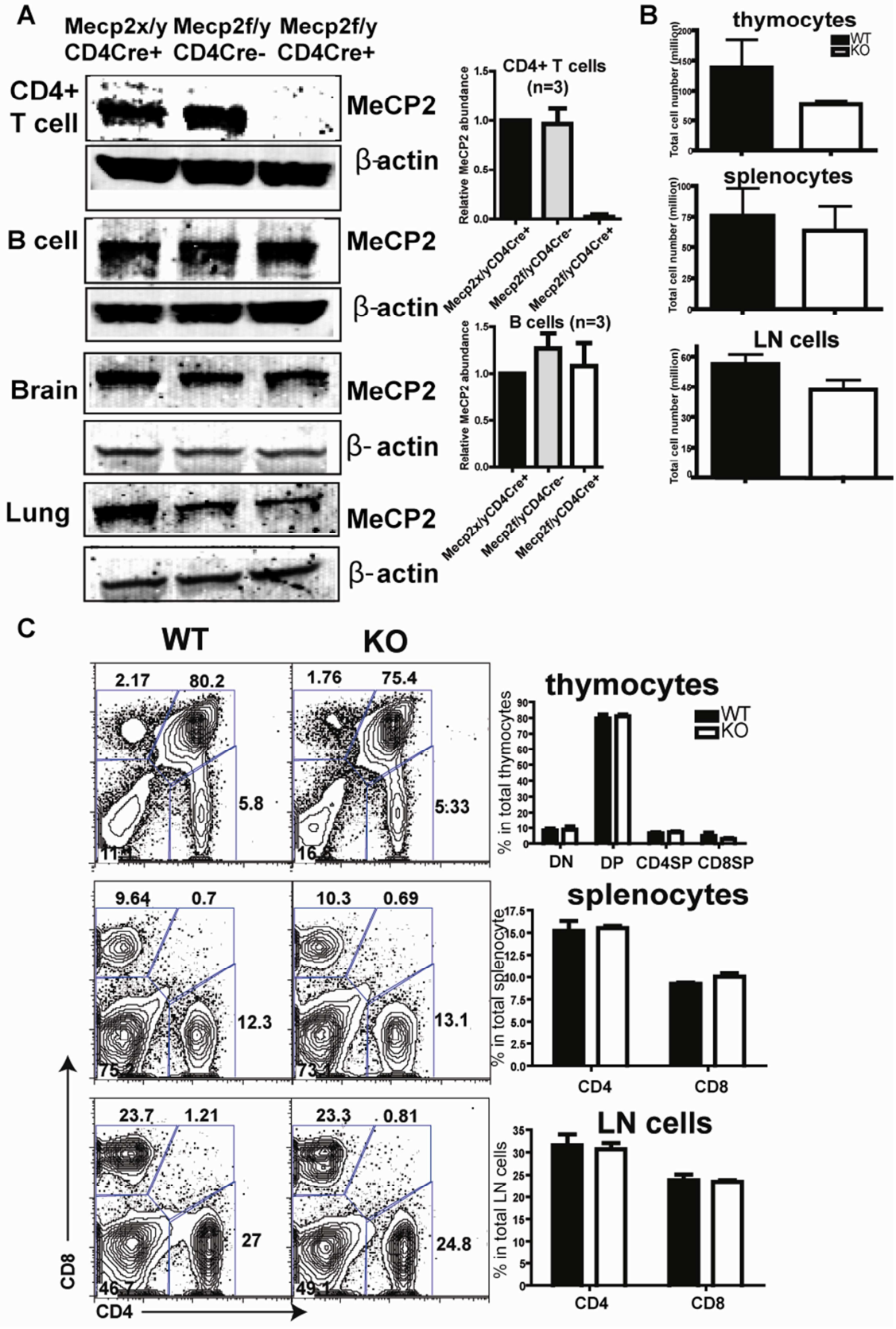
A
Mecp2x/y CD4Cre+
Mecp2f/y CD4Cre-
Mecp2f/y CD4Cre+
CD4+ T cell
MeCP2
β-actin
B cell
Brain
Lung
CD4+ T cells (n=3)
Relative MeCP2 abundance
Mecp2x/yCD4Cre+
Mecp2f/yCD4Cre-
Mecp2f/yCD4Cre+
B cells (n=3)
B
thymocytes
splenocytes
LN cells
WT
KO
Total cell number (million)
C
WT
KO
2.17
80.2
5.8
11.4
1.76
75.4
5.33
16
thymocytes
% in total thymocytes
DN
DP
CD4SP
CD8SP
9.64
0.7
12.3
75
10.3
0.69
13.1
73.1
splenocytes
% in total splenocyte
CD4
CD8
23.7
1.21
27
46.7
23.3
0.81
24.8
49.1
LN cells
% in total LN cells
CD8
CD4

Fig. S1. CD4$^+$ T cell development is normal in mice with T cell–specific deletion of *Mecp2*. (**A**) Naïve CD4$^+$CD25$^-$ T cells and B cells from CD4-Cre$^+$*Mecp2*$^{x/y}$, CD4-Cre$^-$*Mecp2*$^{f/y}$, and CD4-Cre$^+$*Mecp2*$^{f/y}$ littermates were sorted by flow cytometry. The amounts of MeCP2 in these cells and in the brains and lungs of these mice were determined by Western blotting analysis. Blots are representative of three independent experiments. Bar graph shows means ± SEM from three independent experiments. (**B**) Absolute numbers of cells from the thymus, spleen, and lymph nodes (LN) of 6- to 8-week-old CD4-Cre$^+$*Mecp2*$^{x/x}$ or CD4-Cre$^+$*Mecp2*$^{x/y}$ (WT) and CD4-Cre$^+$*Mecp2*$^{f/f}$ or CD4-Cre$^+$*mecp2*$^{f/y}$ (KO) littermates. Pooled data are from five pairs of mouse littermates. Data are means ± SEM. (**C**) Analysis of the percentages of T cells from the thymus, spleen, and lymph nodes of 6- to 8-week-old WT and MeCP2 KO littermates. Left: Representative flow cytometry plots. Right: Pooled data from three pairs of mouse littermates. Data are means ± SEM.

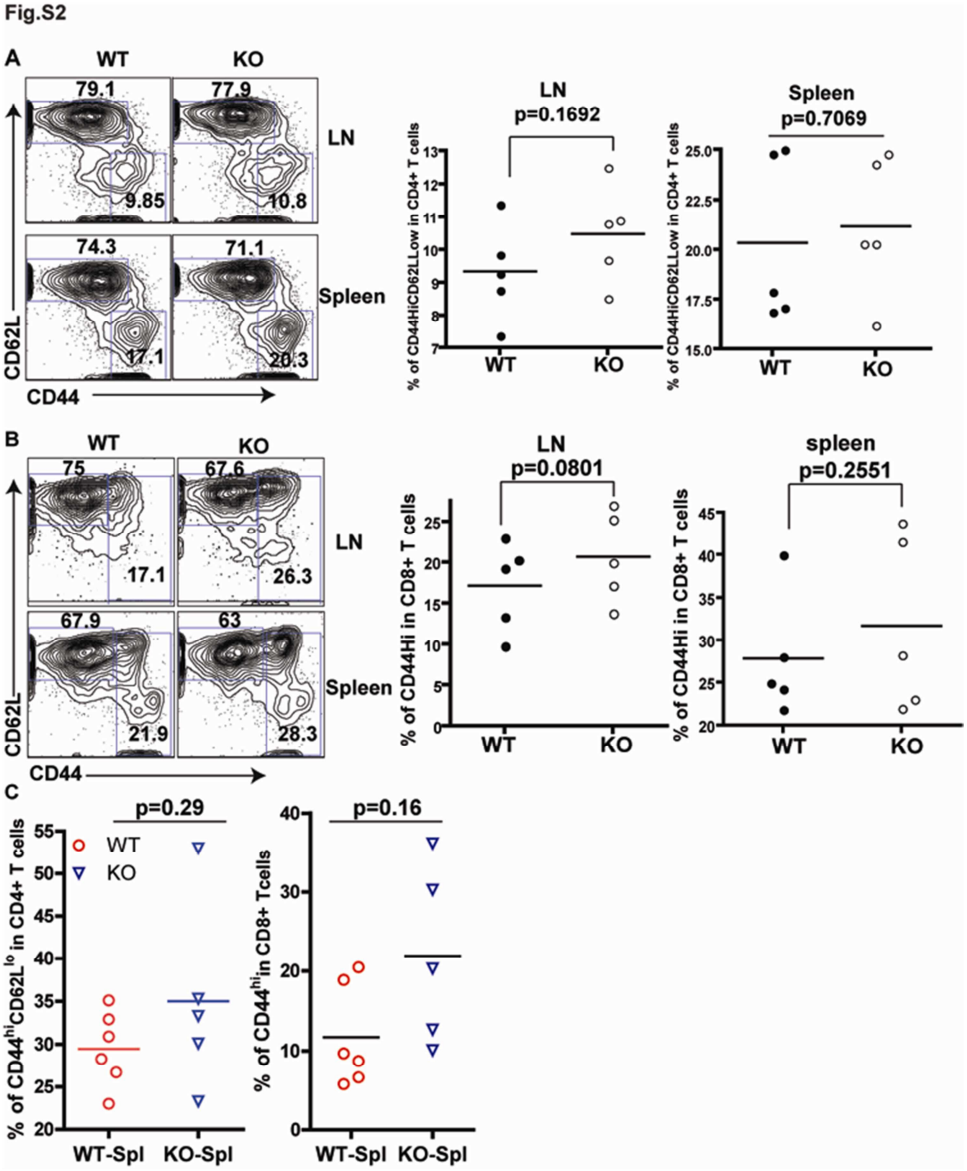

Fig. S2. T cells in *Mecp2*-deficient mice do not undergo spontaneous activation. (**A** and **B**) Flow cytometric analysis of the percentages of effector cells among (A) $CD4^+$ T cells and (B) $CD8^+$ T cells from the lymph nodes (LN) and spleens of 6- to 8-week-old WT and MeCP2 KO littermates. Left: Representative flow cytometry plots. Right: Pooled data are from five pairs of mouse littermates. Data are means and were analysed by student's *t* test results. (**C**) Percentages of effector cells among $CD4^+$ (left) and $CD8^+$ (right) T cells from the spleens of 8- to 14-month-old WT and MeCP2 KO mice. Pooled data present means from six pairs of mouse littermates.

Fig.S3

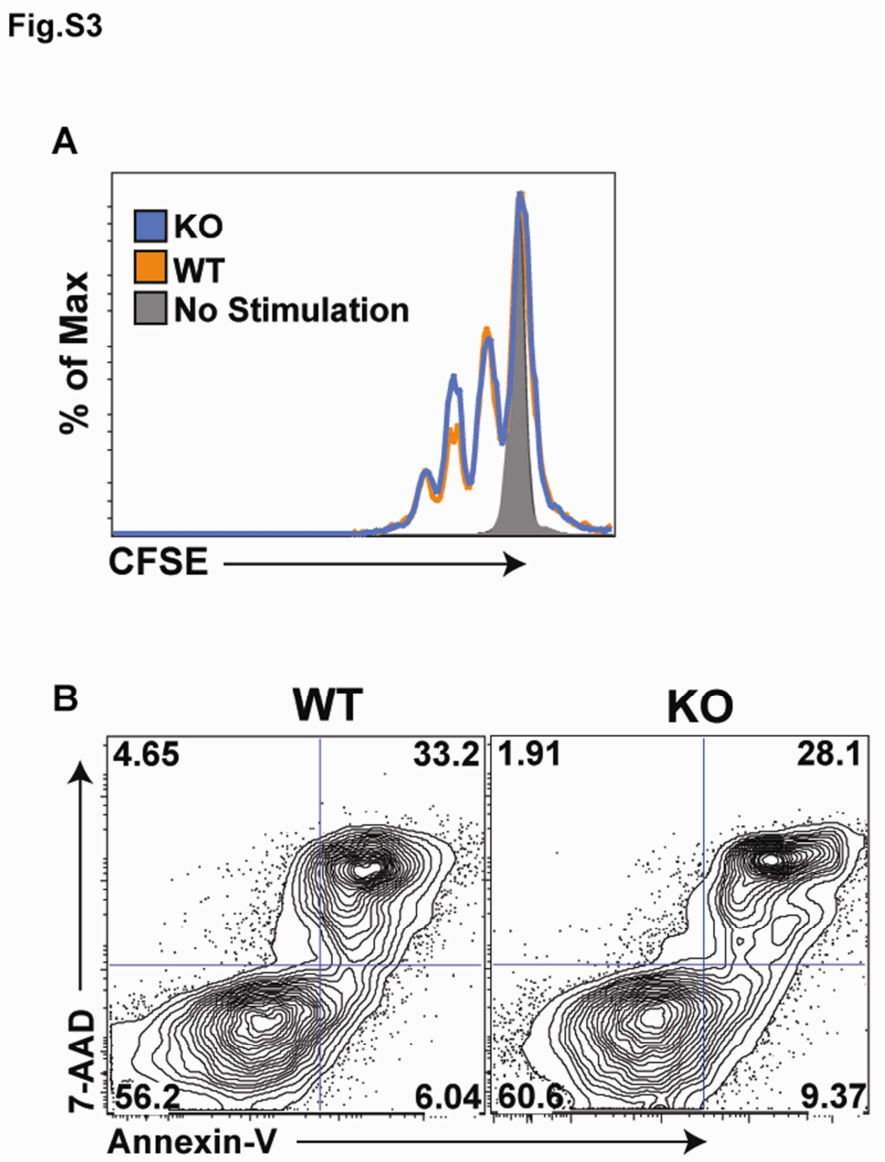

Fig. S3. Loss of MeCP2 does not alter antigen-dependent proliferation or activation-induced cell death. (**A** and **B**) Lymphocytes from LLO118 TCR transgenic WT and MeCP2 KO littermates were labeled with CFSE and primed with 5 μM $LLO_{190-205}$ peptide for 72 hours. (A) Proliferation of $CD4^+$ T cells was measured by flow cytometric analysis of the extent of dilution of CFSE. (B) Activation-induced cell death was assessed by Annexin V and 7-AAD staining. Data are representative of three independent experiments.

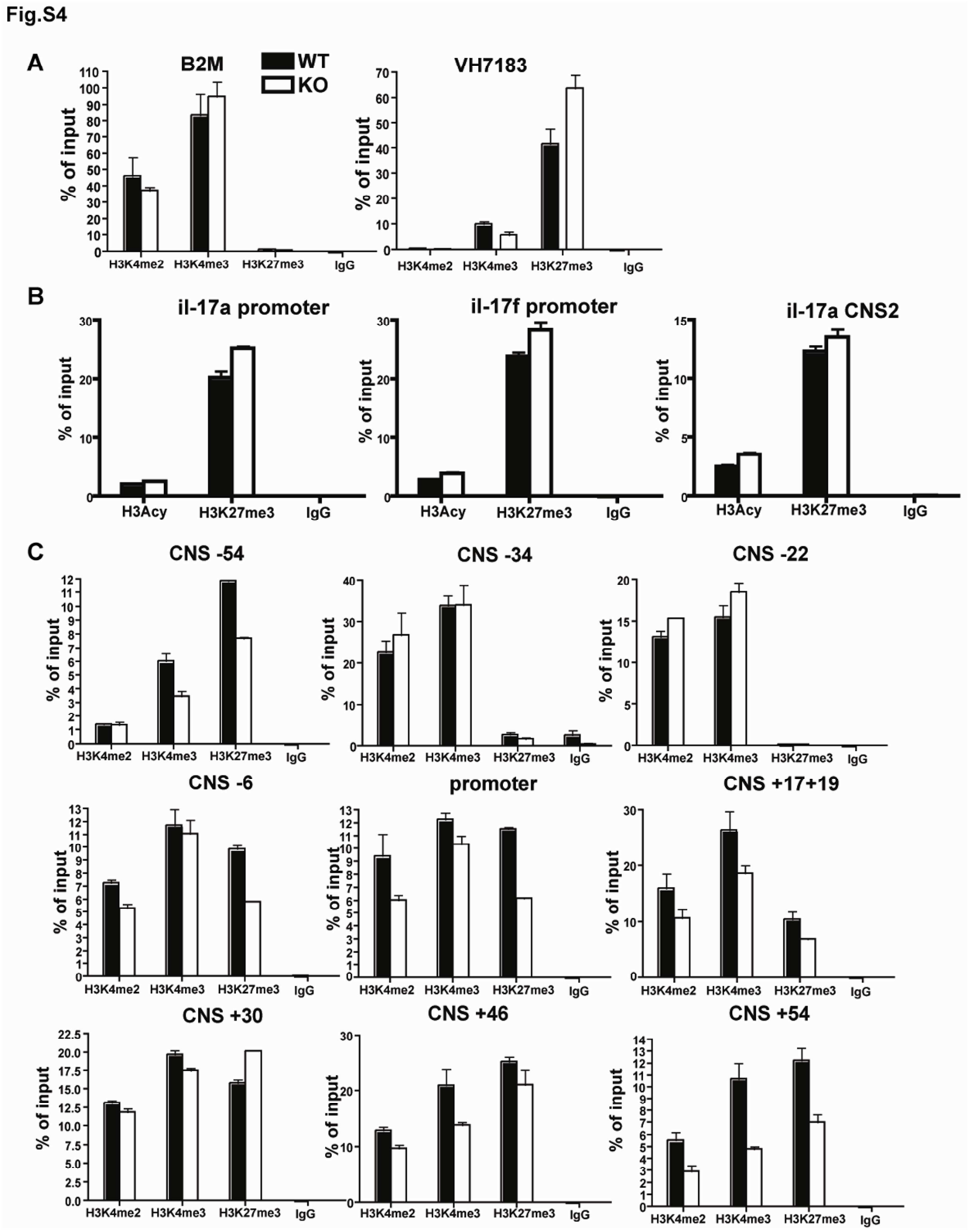

Fig. S4. Chromatin accessibility of the *Il17* and *Ifng* loci in naïve CD4$^+$CD25$^-$ T cells. (**A**) Histone modifications of the *β2m* (B2M) and *vh7183* (VH7183) loci in CD4$^+$ T cells from WT

and MeCP2 KO mice were determined by ChIP assay. (**B** and **C**) Histone modifications of different cis elements within the (B) *Il17* and (C) *Ifng* loci in naïve $CD4^{+}CD25^{-}$ were measured by ChIP analysis. The histone modifications in the *β2m* and *vh7183* loci in $CD4^{+}$ T cells in (A) served as positive and negative controls, respectively. Data are means ± SEM of triplicate samples from a single experiment and are representative of three independent experiments.

Fig. S5

A

JAK and STAT Proteins:	JAK1, JAK2, JAK3, TYK2, STAT1, STAT2, STAT3, STAT4, STAT5A, STAT5B, STAT6.
Receptors that Bind and Activate JAK Proteins:	SH2B2 (APS), FAS (TNFRSF6), IL2RA, IL2RG, IL6ST, PTPRC (CD45), IL6RA, TCF8, ITGA4, CEBPD, RUNX1, RUNX3, CD6, BTG2, IRF2.
SH3 / SH2 Adaptor Protein Activity:	SH2B2 (APS), SIT1, SLA2.
Transcription Factors or Regulators that Interact with STAT Proteins:	IRF1, SLA2, CEBPB, GATA3, NR3C1.
Genes Induced by STAT Proteins:	IRF1, BCL2L1, CDKN1A (P21), FAS (TNFRSF6), SOCS1, IL2RA, GATA3.
Negative Regulators of the JAK/ STAT pathway:	PIAS1, PIAS2, PIAS3, PIAS4, PTPN1, PTPRC (CD45), SOCS1, SOCS2i, SOCS2ii, SOCS3, SOCS4, SOCS5, SOCS7.
Others:	SHP1, SHP2, PTPN2, PTPN22, PTPN13, PTEN,CDC42, RHOA, RAC-1, IL7RA, IL15RA, MCL1, FOXO1, FOXP3, RORC, TBET, IRF4, IRF5, IRF7, IRF9, BCL2, BAX, BAK, UBE3A.

B

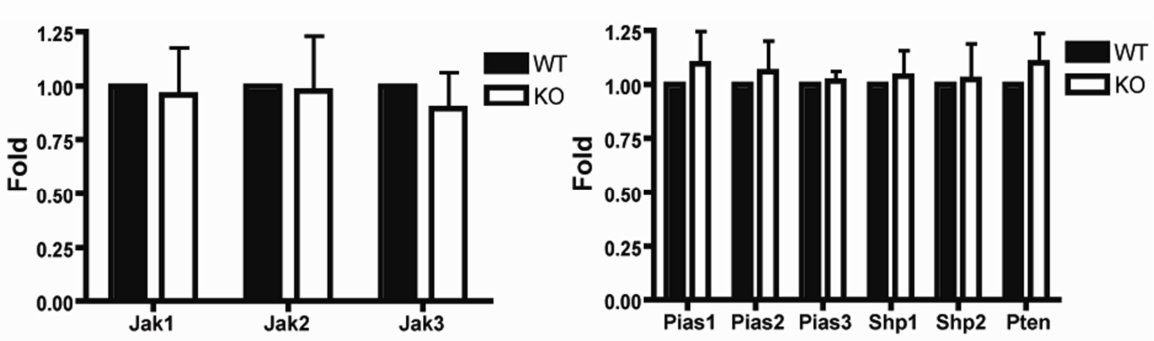

Fig. S5. Abundances of mRNAs for components of STAT signaling pathways. (**A**) List of proteins related to STAT activation whose mRNA amounts were determined by quantitative PCR analysis. (**B**) Fold-differences in the abundances of the indicated mRNAs between WT and MeCP2 KO $CD4^+$ T cells were determined by quantitative PCR analysis. Data are means ± SEM from three independent experiments.

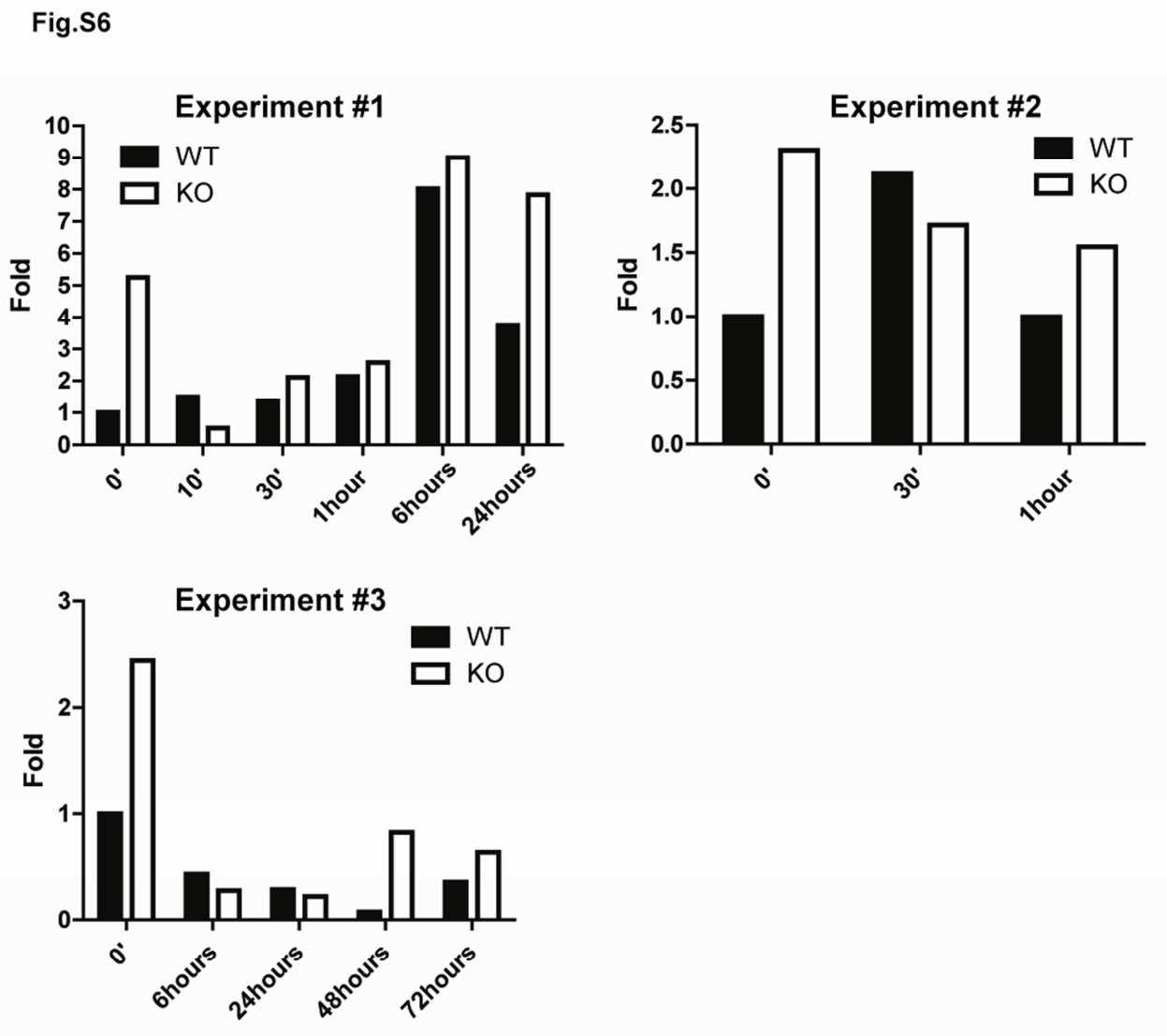

Fig. S6. The dynamics of SOCS5 abundance during the activation of CD4$^+$ T cells in the presence of IL-6. CD4$^+$CD25$^-$ T cells from WT and MeCP2 KO mice were activated in vitro with anti-CD3 and anti-CD28 antibodies in the presence of IL-6 (50 ng/ml) for various times. Amounts of SOCS5 protein were analyzed by Western blotting. The intensities of bands corresponding to SOCS5 were normalized to the intensities of bands corresponding to β-actin, the loading control. For relative quantification, the amounts of SOCS5 protein in WT cells before stimulation (time zero) were set to one. Data from three independent experiments are shown.

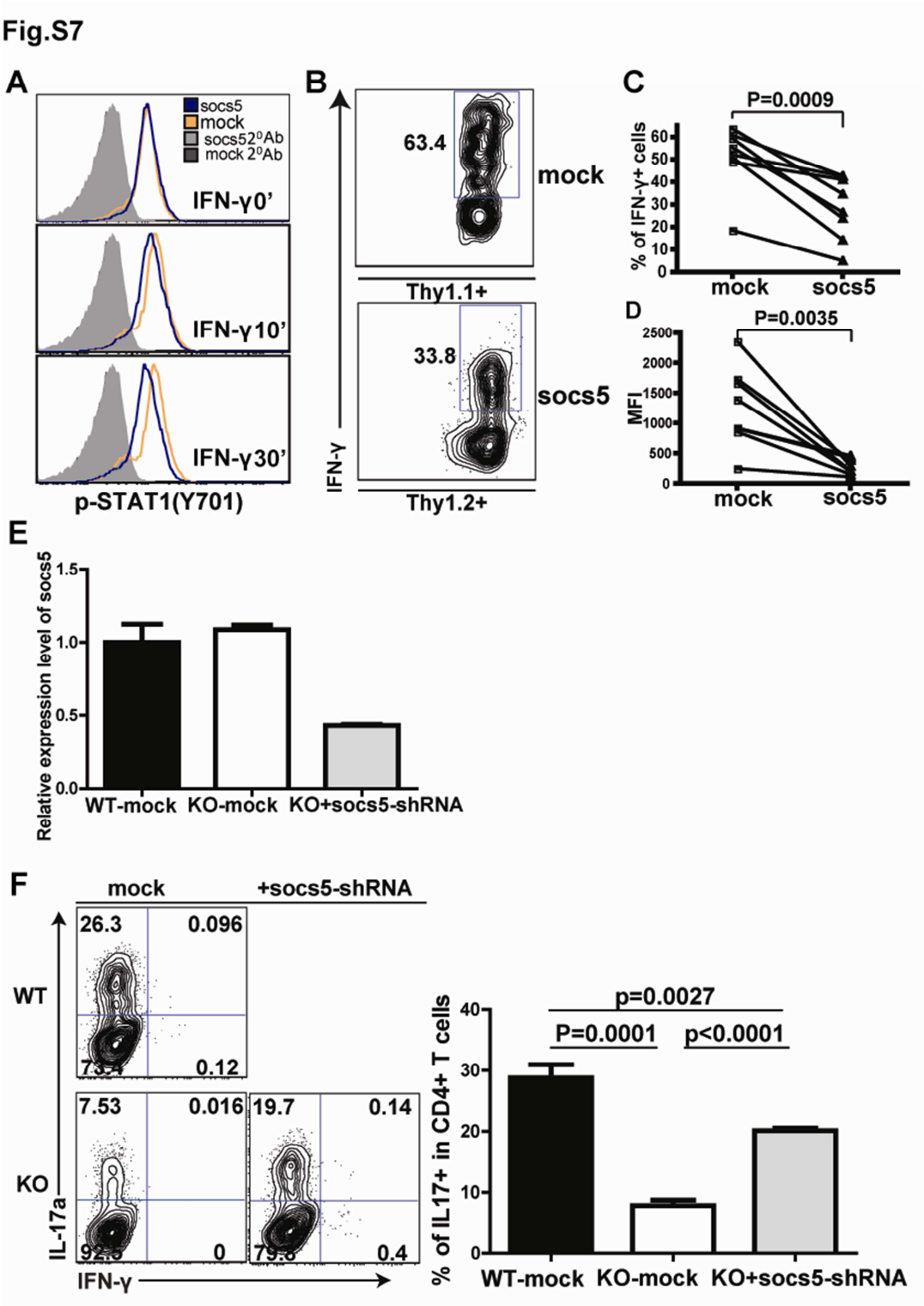

Fig. S7. SOCS5 inhibits the activation of STAT1 and the differentiation of naïve CD4$^+$ T cells. (**A**) CD4$^+$ T cells transduced with control retrovirus expressing GFP or with retrovirus expressing SOCS5 and GFP were treated with IFN-γ (10 ng/ml) for 10 or 30 min, and then the abundance of pSTAT1 (Tyr^{701}) was determined by intracellular staining and flow cytometric

analysis. (**B** to **D**) $CD4^+$ T cells from LLO118 TCR transgenic mice with different Thy markers were transduced with retroviruses expressing either GFP (Thy1.1+) or SOCS5 (Thy1.2+). Six hours after competitive transfer of control and SOCS5-expressing ($CD4^+GFP^+$) cells in a ratio of 1:1 to $TCR\alpha^{-/-}$ recipient mice (n = eight mice), the recipient mice were immunized subcutaneously with $LLO_{190\text{-}205}$ peptide emulsified in CFA. Five days after immunization, splenocytes from the recipient mice were rechallenged with $LLO_{190\text{-}205}$ peptide and were cultured under T_H1-skewing conditions in vitro. Forty-eight hours later, IFN-γ–producing GFP^+CD4^+ T cells were enumerated by intracellular staining and flow cytometric analysis. (B) Representative flow cytometry contour plots. (C) Percentages of IFN-γ^+ cells. (D) MFIs of IFN-γ staining. Graph represents two independent experiments. (**E** and **F**) Lymphocytes from LLO118 TCR transgenic WT and MeCP2 KO mice were transduced with control retrovirus or with retrovirus expressing *Socs5*-specific shRNA. (E) Total RNA was isolated from GFP^+CD4^+ T cells from the indicated samples, and the amount of *Socs5* mRNA was determined by quantitative PCR analysis. (F) $CD4^+$ T cells from LLO118 TCR transgenic WT and MeCP2 KO littermates were cultured under T_H17-skewing conditions. Four days after retroviral infection, IL-17A production in $CD4^+GFP^+$ T cells was detected by intracellular staining and flow cytometric analysis. Left: Percentages of IL-$17A^+$ cells among $CD4^+$ cells from the indicated conditions. Right: Mean percentages ± SEM of IL-17^+ cells from three independent experiments.

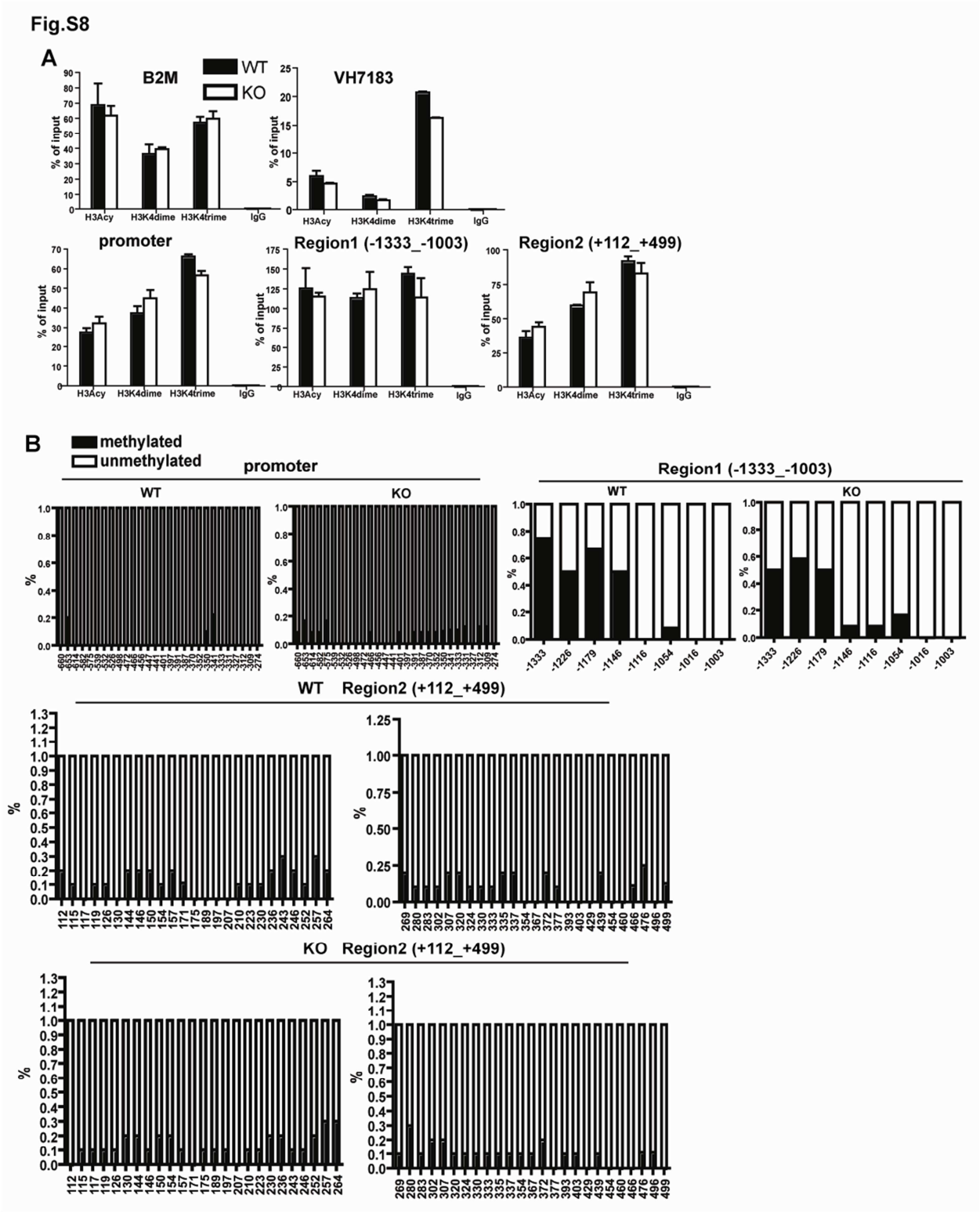

Fig. S8. The chromatin accessibility of the *Socs5* locus in naïve CD4^{+}CD25^{-} T cells. (**A**) ChIP analysis of the histone modifications of different cis elements within the *Socs5* locus in

naïve $CD4^{+}CD25^{-}$ T cells from WT and MeCP2 KO mice. Data are means ± SEM of triplicate samples from a single experiment and are representative of three independent experiments. ChIP analyses of *B2m* and *Vh7183* were performed as controls. (**B**) Analysis of the methylation status in the promoter and the conserved noncoding sequence (CNS) of *Socs5* locus by bisulfite sequencing. Numbers on the x-axes indicate the position of CpG islands relative to the transcription start site of *Socs5*. Bar graphs show data quantified from the sequencing of at least ten clones for each sample. Data are representative of three independent experiments.

Fig.S9

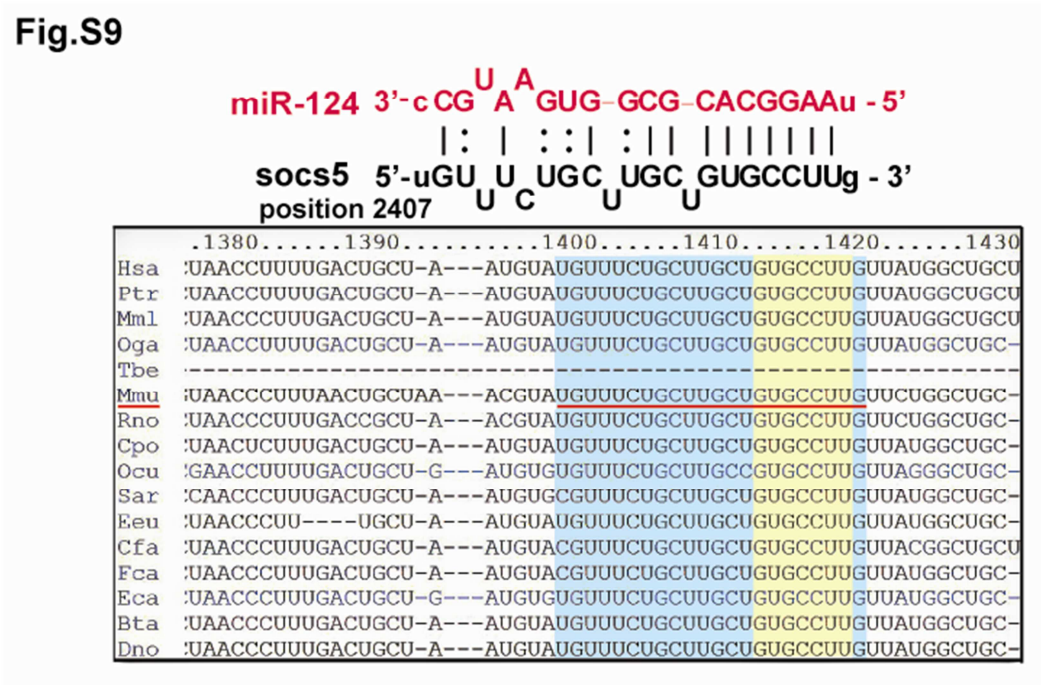

Fig. S9. miR-124 was computationally predicted to target *Socs5* mRNA at a highly conserved site. Top: Schematic representation of the putative miR-124–binding site within the 3′UTR of *Socs5*. Bottom: The sequences of the 3′UTRs of *Socs5* from different species, which contain the indicated miR-124–binding site. Nucleotides that are complimentary to the seed region (nucleotides 2-8) of miR-124 are shown in yellow; nucleotides predicted to interact with the rest of miR-124 are shown in blue. The red line underscores the mRNA of mouse *Socs5*.

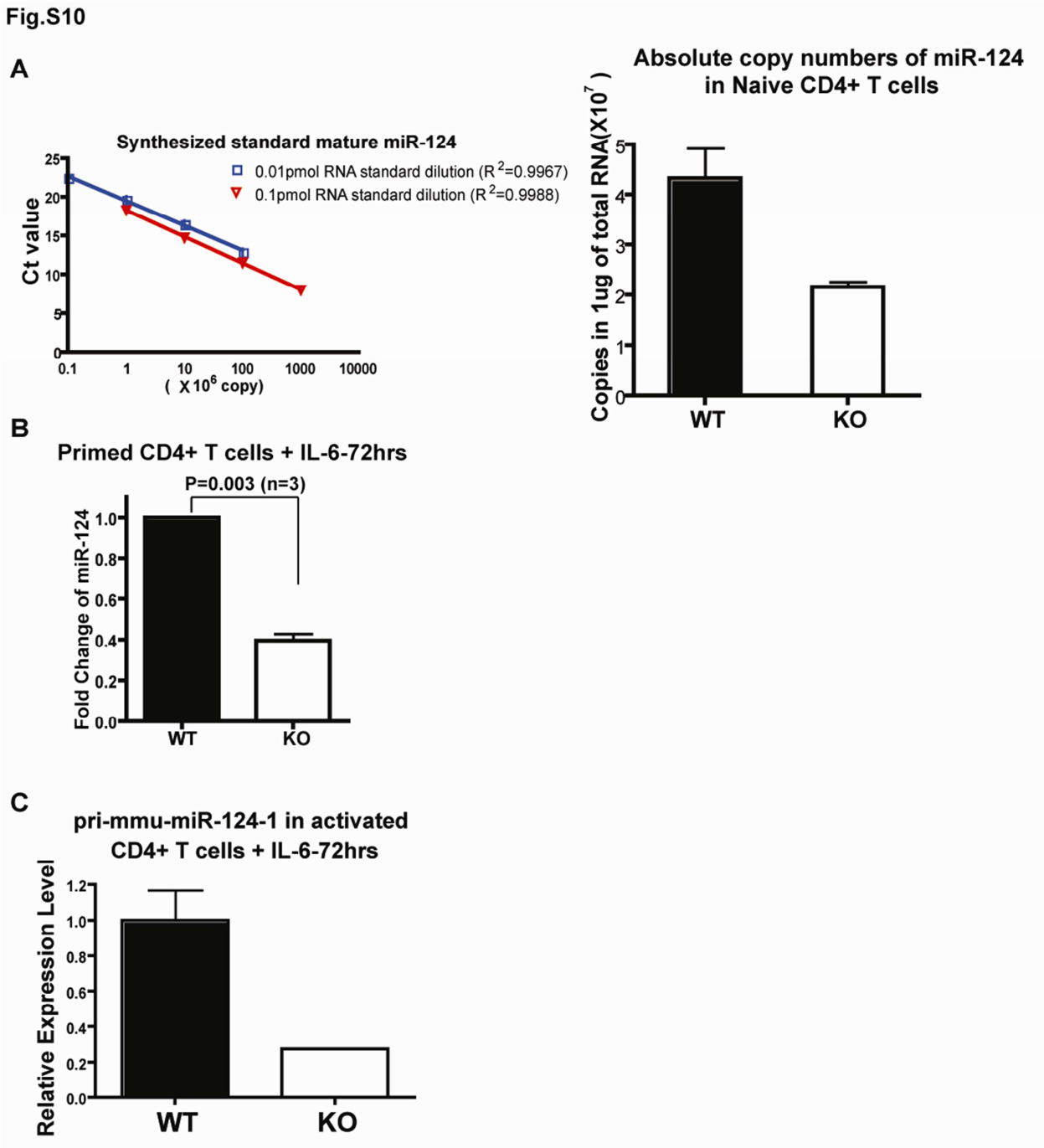

Fig. S10. Activated MeCP2-deficient CD4$^+$ T cells have decreased amounts of pri-miR-124 and mature miR-124 compared to those of wild-type CD4$^+$ T cells. (**A**) Left: Standard curves for calculating the absolute copy numbers of mature miR-124. Synthesized standard mature miR-124 (0.1 or 0.01 pmol) was processed to cDNA through reverse transcription. The cDNAs generated were further diluted before they were analyzed by quantitative PCR. Linear regression [y:Ct value; x:log10(copy numbers per PCR reaction)-5] was used to calculate the standard curve. Right: The absolute copy numbers of miR-124 in naïve CD4$^+$ T cells from WT and MeCP2 KO mice were determined by quantitative PCR analysis. (**B**) Total RNA from CD4$^+$CD25$^-$ T cells

from WT and MeCP2 KO mice were primed with anti-CD3 and anti-CD28 antibodies together with IL-6 for 72 hours. Total RNA was then extracted, and the amounts of miR-124 were determined by quantitative PCR analysis. Data are means ± SEM from three independent experiments. (**C**) The relative amounts of pri-mmu-miR-124-1 transcripts in primed $CD4^{+}CD25^{-}$ T cells from WT and MeCP2 KO mice were determined by quantitative PCR analysis. Data are means ± SEM from three replicated samples and represent three independent experiments.

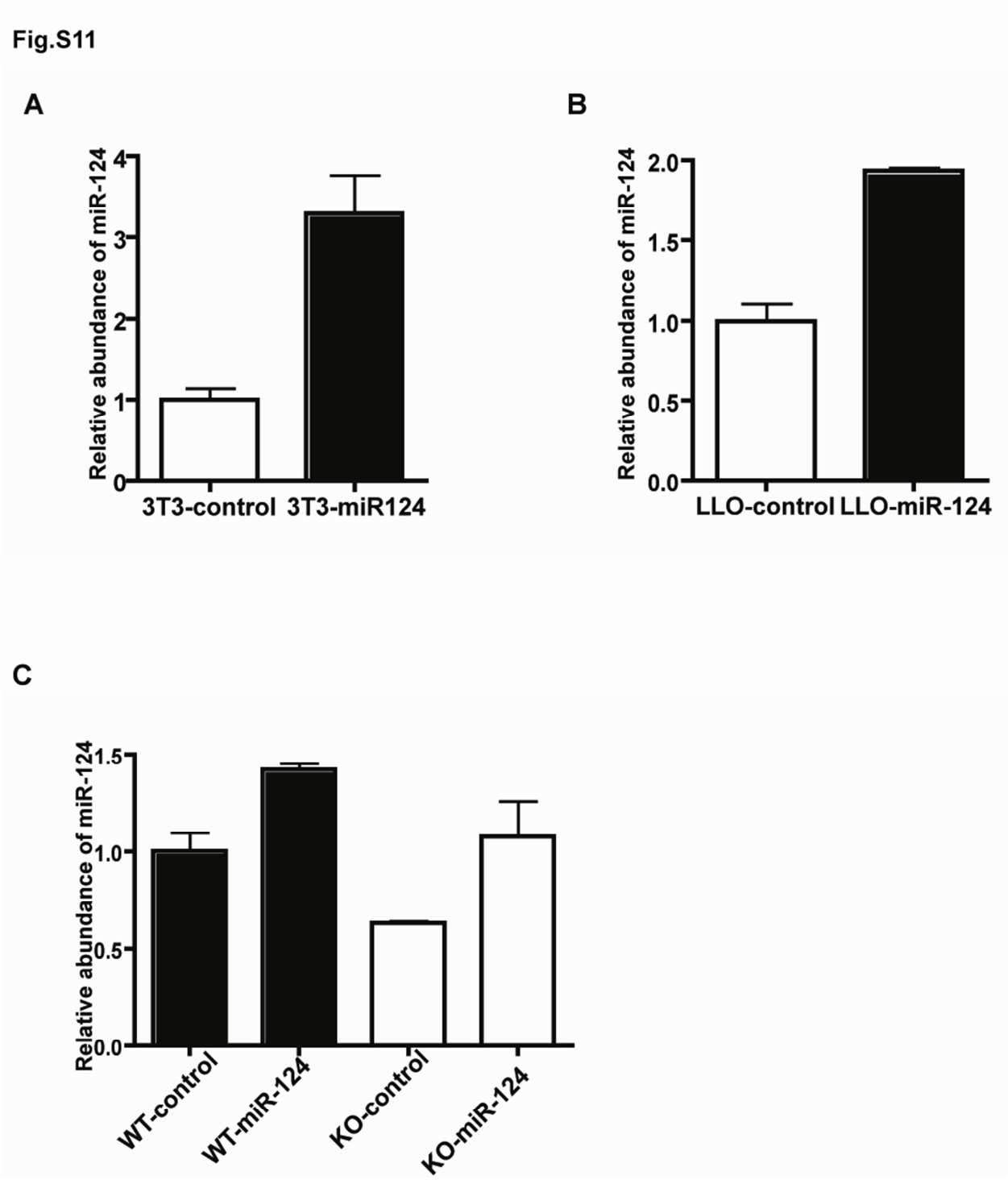

Fig. S11. Retroviral-mediated overexpression of miR-124 in 3T3 cells and CD4$^+$ T cells. (**A**) The relative abundances of miR-124 in the indicated 3T3 stable cell lines were measured by quantitative PCR analysis. Data are means ± SEM from three biological replicates and represent three independent experiments. (**B**) Lymphocytes from LLO118 TCR transgenic mice were transduced with control retrovirus or with retrovirus expressing miR-124. Seventy-two hours after infection, CD4$^+$GFP$^+$ T cells were sorted by flow cytometry and their relative abundances

of miR-124 were measured by quantitative PCR analysis. Data are means ± SEM from three biological replicates and represent three independent experiments. (**C**) Lymphocytes from LLO118 TCR transgenic WT and MeCP2 KO littermate were transduced with control retrovirus or with retrovirus expressing miR-124. Seventy-two hours later, $CD4^{+}GFP^{+}$ T cells were sorted by flow cytometry, and their relative abundances of miR-124 were determined by quantitative PCR analysis. Data are means ± SEM from three biological replicates and represent three independent experiments.

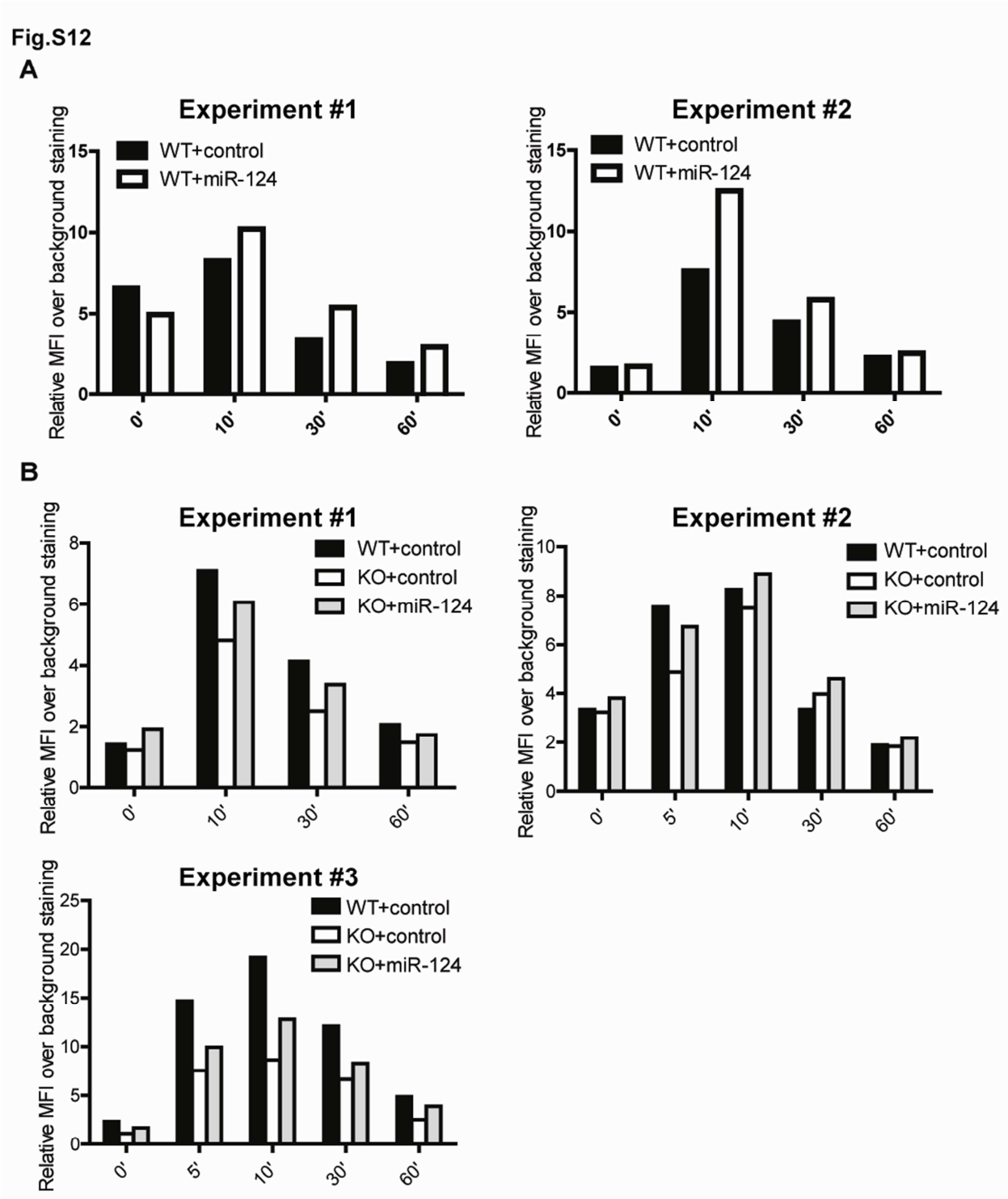

Fig. S12. miR-124 promotes IL-6–induced STAT3 activation in CD4$^+$ T cells. (**A**) The MFI quantification of pSTAT3 (Tyr^{705}) staining for Fig. 7D. (**B**) The MFI quantification of pSTAT3 (Tyr^{705}) staining for Fig. 7E. Data were normalized to the background signal with the secondary antibody staining.

Fig. S13

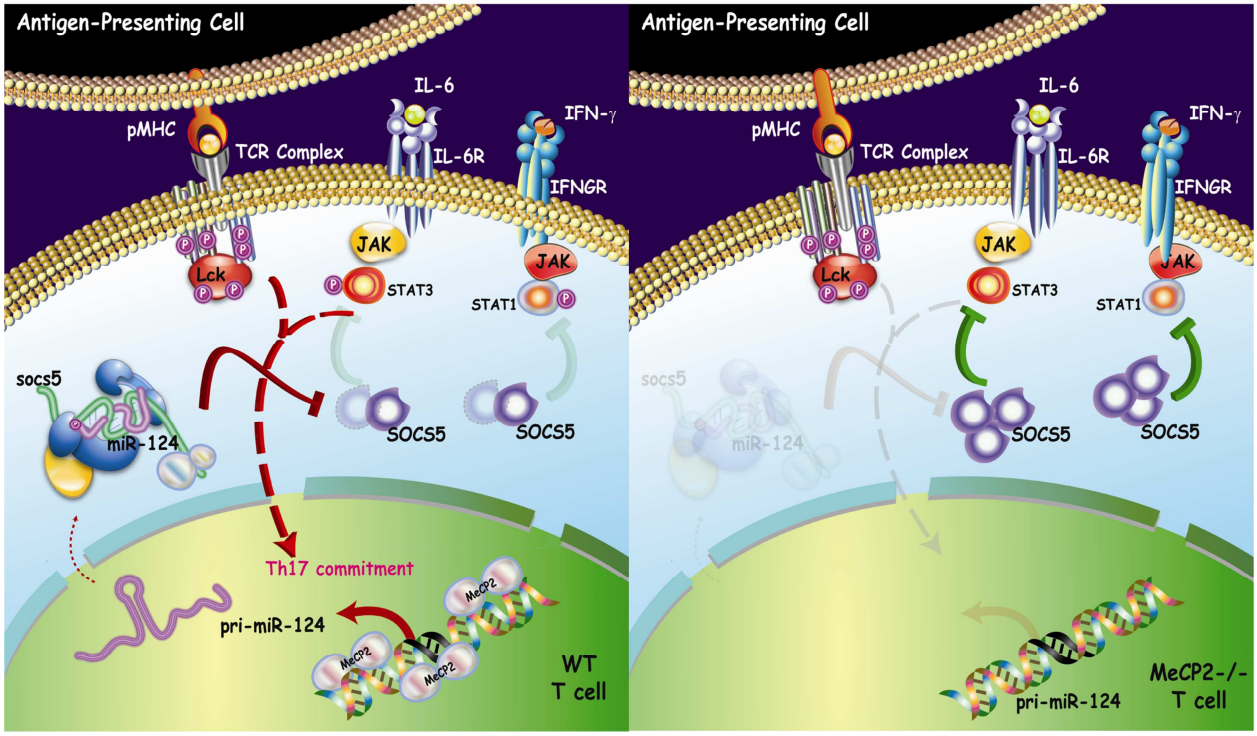

Fig. S13. The MeCP2–miR-124–SOCS5 axis enables CD4$^+$ T cell differentiation. Left: In WT CD4$^+$ T cells, MeCP2 promotes the transcription of *pri-miR-124*, which results in the suppression of *Socs5* expression. Loss of SOCS5 enables the efficient differentiation of naïve CD4$^+$ T cells into T_H17 cells. Right: In MeCP2-deficient CD4$^+$ T cells, the accumulation of SOCS5 protein results in the attenuation of STAT3 signaling, which impairs the generation of T_H17 cells.

Fig.S14

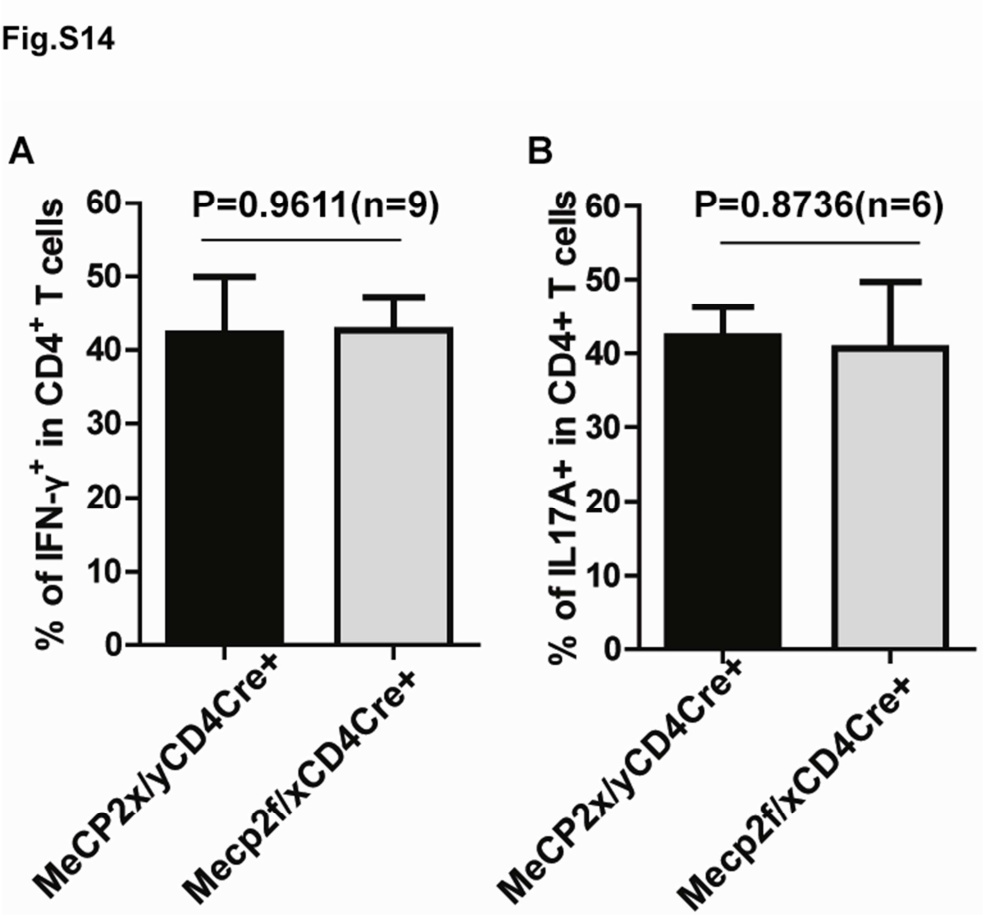

Fig. S14. Loss of a single copy of *Mecp2* does not adversely affect the generation of T_H1 and T_H17 mouse T cells. (**A** and **B**) T cells from LLO118 TCR transgenic WT mice and littermates with heterozygous *Mecp2* deletion were cultured in vitro under T_H1- or T_H17-skewing conditions for 4 days. The percentages of (A) IFN-γ–producing and (B) IL-17A–producing $CD4^+$ T cells were determined by flow cytometric analysis. Data are means ± SEM from the indicated numbers of experiments.